Directed searches for continuous gravitational waves from twelve supernova remnants in data from Advanced LIGO's second observing run

Lee Lindblom

Center for Astrophysics and Space Sciences, University of California at San Diego, La Jolla, California 92093-0424, USA

Benjamin J. Owen

Department of Physics and Astronomy, Texas Tech University, Lubbock, Texas 79409-1051, USA

(Received 28 February 2020; accepted 27 March 2020; published 16 April 2020)

We describe directed searches for continuous gravitational waves from twelve well-localized nonpulsing candidate neutron stars in young supernova remnants using data from Advanced LIGO's second observing run. We assumed that each neutron star is isolated and searched a band of frequencies from 15 to 150 Hz, consistent with frequencies expected from known young pulsars. After coherently integrating spans of data ranging from 12.0 to 55.9 days using the $\mathcal{F}$-statistic and applying data-based vetoes, we found no evidence of astrophysical signals. We set upper limits on intrinsic gravitational wave amplitude in some cases stronger than 10^{-25}, generally about a factor of two better than upper limits on the same objects from Advanced LIGO's first observing run.

DOI: 10.1103/PhysRevD.101.083023

I. INTRODUCTION

Young isolated neutron stars and suspected locations of the same are promising targets for directed searches for continuous gravitational waves (GWs) [1]. Even without timing obtained from electromagnetic observations of a pulsar, such searches can achieve interesting sensitivities for reasonable computational costs [2]. Young supernova remnants (SNRs) containing candidate nonpulsing neutron stars are natural targets for such searches, as are small SNRs or pulsar wind nebulae even in the absence of a candidate neutron star (as long as the SNR is not Type Ia, which does not leave behind a compact object).

Many upper limits on continuous GWs from isolated, well-localized neutron stars other than known pulsars have been published over the last decade. These have used data ranging from Initial LIGO runs to Advanced LIGO's first observing run (O1) and second observing run (O2). Most searches targeted relatively young SNRs [3–11]. Some searches targeted promising small areas such as the galactic center [4,8,11–13]. One search targeted a nearby globular cluster, where multibody interactions might effectively rejuvenate an old neutron star for purposes of continuous GW emission [14]. Some searches used short coherence times and fast, computationally cheap methods originally developed for the stochastic GW background [4,8,11]. Most searches were slower but more sensitive, using longer coherence times and methods specialized for continuous waves based on matched filtering and similar techniques.

Here we present the first searches of O2 data for twelve SNRs, using the fully coherent $\mathcal{F}$-statistic as implemented in a code pipeline descended from the one used in the first published search [3] among others [5,9]. Since the O2 noise spectrum is not much lower than O1, we deepened these searches with respect to O1 searches [9] by focusing on low frequencies compatible with those observed in young pulsars [15]. This focus allowed us to increase coherence times and obtain significant improvements in sensitivity over O1. Low frequencies have the drawback, however, that greater neutron star ellipticities or r-mode amplitudes are required to generate detectable signals. We did not search three SNRs from the list in Ref. [9] because the Einstein@Home distributed computing project has already searched them [10] to a depth which cannot be matched without such great computing resources which we do not have. We also did not search Fomalhaut b as in Ref. [9] because our code (although improved over previous versions) is inefficient for targets with such long spin-down timescales. In the future we plan to improve the code to efficiently search higher frequencies and longer spin-down timescales. For now our searches are interesting as the most sensitive yet (in strain) for these twelve SNRs.

II. SEARCHES

In most respects the searches were done similarly to [9], so we summarize briefly and refer the reader to that paper for further details. The same goes for the upper limits described in the next section.

A. Setup

We made the usual assumptions about the signals, that they had negligible intrinsic amplitude evolution and that their frequency evolution in the frame of the solar system barycenter was given by

$$f(t) = f + \dot{f}(t - t_0) + \frac{1}{2}\ddot{f}(t - t_0)^2, \tag{1}$$

where t_0 is the beginning of the observation, the frequency derivatives are evaluated at that time, and we write a simple f for $f(t_0)$. Hence our searches were sensitive to neutron stars without binary companions, significant timing noise, or glitches; and spinning down on timescales much longer than the duration of any observation.

We used the multidetector $\mathcal{F}$-statistic [16,17], which combines matched filters for the above type of signal in such a way as to account for amplitude and phase modulation due to the daily rotation of the detectors with relatively little computational cost. In stationary Gaussian noise, $2\mathcal{F}$ is drawn from a χ^2 distribution with four degrees of freedom. The χ^2 is noncentral if a signal is present. For loud signals the amplitude signal-to-noise ratio is roughly $\sqrt{\mathcal{F}/2}$.

We used Advanced LIGO O2 data [18,19] with version `C02` calibration and cleaning as described in [20]. Thus the amplitude calibration uncertainties were no greater than 8% for each interferometer. As in previous searches of this type, we used strain data processed into short Fourier transforms (SFTs) of 1800 s duration, high pass filtered and Tukey windowed. And we chose the set of SFTs for each search, once its time span was fixed (see below), by minimizing the harmonic mean of the noise power spectral density over the span and the frequency band.

With the direction to each candidate neutron star known, the parameter space of each search was the set $(f, \dot{f}, \ddot{f})$. In contrast to Ref. [9] and earlier searches, we fixed $f_{\min}$ and $f_{\max}$ at 15 Hz and 150 Hz respectively. Our goal was to improve the sensitivity significantly over earlier O1 results [9,10], even though the strain noise was only slightly improved, while focusing on a range of frequencies compatible with the emission expected from known young pulsars [15]. Rounding up a bit from the 124 Hz expected from the fastest known young pulsar, we set $f_{\max}$ to 150 Hz. Since the precise value of $f_{\min}$ has very little effect on the cost of the searches, we somewhat arbitrarily set it to 15 Hz where the noise spectrum is rising steeply. The ranges of frequency derivatives were then chosen as in [9], with

$$-\frac{f}{a} \le \dot{f} \le -\frac{1}{6}\frac{f}{a} \tag{2}$$

for a given f and

$$2\frac{\dot{f}^2}{f} \le \ddot{f} \le 7\frac{\dot{f}^2}{f} \tag{3}$$

for a given $(f, \dot{f})$. Thus we were open to a wide but physically motivated range of possible emission scenarios.

B. Target list

Our choice of targets was based on the same criteria adopted in the O1 search [9]. We required that our search of a particular target at fixed computational cost be sensitive enough to detect the strongest continuous GW signal consistent with conservation of energy. This strongest signal, based on the age a and distance D of the source,

$$h_0^{\text{age}} = 1.26 \times 10^{-24}\left(\frac{3.30\ \text{kpc}}{D}\right)\left(\frac{300\ \text{yr}}{a}\right)^{1/2}, \tag{4}$$

is analogous to the spin-down limit for known pulsars and indicates the strongest possible intrinsic amplitude produced by an object whose unknown spin-down is entirely due to GW emission and has been since birth [2]. The intrinsic amplitude h_0 characterizes the GW metric perturbation without reference to any particular orientation or polarization [16], and therefore is typically a factor 2–3 larger than the actual strain response of the interferometers.

As in the O1 search [9] we selected targets from Green's catalog of SNRs [21] (now the 2019 version). We focused on very small young remnants and those containing x-ray point sources or small pulsar wind nebulae. We selected only those SNRs with age and distance estimates resulting in h_0^{age} large enough to be detectable within our computing budget (see below). In addition to the Green SNRs we included the candidate SNR G354.4 + 0.0 [22] as in Ref. [9], although a recent multiinstrument comparison [23] argues that it is probably an HII region. As in Ref. [9], we included SNR G1.9 + 0.3 although it is probably Type Ia. On the scale of our analysis, including two targets which might not contain neutron stars added relatively little to the computational cost.

This process yielded the same 15 SNRs studied in the O1 search [9]. We did not perform searches on G111.7 − 2.1, G266.2 − 1.2, and G347.3 − 0.5 from that target list since they had already been searched [10] with greater sensitivity than we could achieve with our more limited computational resources. The resulting targets for our searches, along with the sources of their key astrophysical parameters, are given in Table I. Table II summarizes various derived parameters used in our searches of these targets. Brief descriptions and more details on the provenance of parameters are given in [9]. For four targets we ran "wide" and "deep" searches based on optimistic and pessimistic estimates of age and distance from the literature, and thus we had 16 searches for 12 SNRs. (Although the wide and deep searches cover the same frequencies, they cover ranges of spin-down parameters that usually have little to no overlap.) For G15.9 + 0.2

TABLE I. Astronomical parameters of SNRs used in each search: Right ascension and declination, distance D, age a, and references for each parameter. For SNRs whose range of age and distance estimates in the literature is not too great, the search used the optimistic (nearby and young) end of the range. For some SNRs the range was great enough to justify separate wide parameter searches (optimistic) and deep parameter searches (pessimistic).

SNR (G name)	Parameter space	Other name	RA + dec (J2000 h:m:s + d:m:s)	Ref.	D (kpc)	Ref.	a (kyr)	Ref.
1.9 + 0.3		···	17:48:46.9 − 27:10:16	[24]	8.5	[25]	0.1	[25]
15.9 + 0.2	Wide	···	18:18:52.1 − 15:02:14	[26]	8.5	[26]	0.54	[26]
15.9 + 0.2	Deep	···	18:18:52.1 − 15:02:14	[26]	8.5	[26]	2.4	[26]
18.9 − 1.1		···	18:29:13.1 − 12:51:13	[27]	2	[28]	4.4	[28]
39.2 − 0.3		3C 396	19:04:04.7 + 05:27:12	[29]	6.2	[30]	3	[30]
65.7 + 1.2		DA 495	19:52:17.0 + 29:25:53	[31]	1.5	[32]	20	[33]
93.3 + 6.9		DA 530	20:52:14.0 + 55:17:22	[34]	1.7	[35]	5	[34]
189.1 + 3.0	Wide	IC 443	06:17:05.3 + 22:21:27	[36]	1.5	[37]	3	[38]
189.1 + 3.0	Deep	IC 443	06:17:05.3 + 22:21:27	[36]	1.5	[37]	20	[39]
291.0 − 0.1		MSH 11 − 62	11:11:48.6 − 60:39:26	[40]	3.5	[41]	1.2	[40]
330.2 + 1.0	Wide	···	16:01:03.1 − 51:33:54	[42]	5	[43]	1	[44]
330.2 + 1.0	Deep	···	16:01:03.1 − 51:33:54	[42]	10	[43]	3	[45]
350.1 − 0.3		···	17:20:54.5 − 37:26:52	[46]	4.5	[46]	0.6	[47]
353.6 − 0.7		···	17:32:03.3 − 34:45:18	[48]	3.2	[49]	27	[49]
354.4 + 0.0	Wide	···	17:31:27.5 − 33:34:12	[22]	5	[22]	0.1	[22]
354.4 + 0.0	Deep	···	17:31:27.5 − 33:34:12	[22]	8	[22]	0.5	[22]

and G330.2 + 1.0 the deep searches were new—the O1 searches could meet the sensitivity goal only for the optimistic estimates, but O2 data allowed us to meet it even for pessimistic estimates.

Consistency checks on the parameters used were much easier than in Ref. [9]. Here we used $f_{\max}$ of 150 Hz, lower than in previous searches of this type. Hence errors due to neglect of higher frequency derivatives and other approximations were reduced by a factor of a few to orders of magnitude over previous searches, and were completely negligible.

C. Computations

Our searches used code descended from the pipeline used in some LIGO searches [3,5,9] whose workhorse is the $\mathcal{F}$-statistic as implemented in the `S6SNRSearch` tag of the LALSUITE software package [50]. Search pipeline

TABLE II. Derived parameters used in each search. The duty factor is the total SFT time divided by T_{span} divided by the number of interferometers (two). As in the previous table, for objects with two entries the first is a wide search (optimistic parameter estimates) and the second is a deep search (pessimistic parameter estimates). The ranges used for the spin-down parameters (described in the text) for wide and deep searches are not the same.

SNR (G name)	Parameter space	T_{span} (seconds)	T_{span} (days)	Start of span (UTC, 2017)	H1 SFTs	L1 SFTs	Duty factor	h_0^{age} ($\times 10^{-25}$)
1.9 + 0.3		1,036,229	12.0	Jun 23 03:59:29	460	466	0.80	8.5
15.9 + 0.2	Wide	1,744,260	20.2	Aug 04 21:11:52	753	748	0.77	3.6
15.9 + 0.2	Deep	2,593,109	30.0	Jul 26 21:41:05	1076	1095	0.75	1.7
18.9 − 1.1		3,014,418	34.9	Jul 22 00:39:16	1204	1272	0.74	5.4
39.2 − 0.3		2,734,846	31.7	Jul 23 17:19:34	1106	1152	0.74	2.1
65.7 + 1.2		4,450,430	51.5	Jan 19 08:03:58	1916	1580	0.71	3.4
93.3 + 6.9		3,067,958	35.5	Jul 21 08:46:56	1224	1288	0.74	6.0
189.1 + 3.0	Dide	2,739,425	31.7	Jul 23 16:03:15	1108	1154	0.74	8.8
189.1 + 3.0	Deep	4,468,104	51.7	Jan 19 03:09:24	1917	1588	0.71	3.4
291.0 − 0.1		2,160,350	25.0	Jul 28 03:45:55	906	913	0.76	5.9
330.2 + 1.0	Wide	2,056,663	23.8	Aug 02 00:41:51	876	865	0.73	4.6
330.2 + 1.0	Deep	2,765,446	32.0	Jul 23 08:49:34	1116	1169	0.74	1.3
350.1 − 0.3		1,794,825	20.8	Aug 05 03:25:49	777	773	0.78	6.5
353.6 − 0.7		4,827,338	55.9	Jul 01 01:03:56	1581	1955	0.66	1.4
354.4 + 0.0	Wide	1,040,749	12.0	Jun 23 02:59:29	462	469	0.81	14.4
354.4 + 0.0	Deep	1,694,450	19.6	Aug 05 03:32:02	736	722	0.77	4.0

improvements mainly consisted of "internal" issues such as better use of disk space, better error tracking, and improved interaction with the batch job queuing system to reduce human workload. Some significant bugs and issues were also addressed, as described below.

All searches ran on the Broadwell Xeon processors of the Quanah computing cluster at Texas Tech. Integration spans were adjusted by hand so that each search took approximately 10^5 core-hours, split into 10^4 batch jobs. Due to the frequency band used for the searches, which avoided the worst spectrally disturbed bands, the total search output used less than one terabyte of disk space.

D. Postprocessing

As in the O1 search [9], post-processing of search results started with the "Fscan veto" and interferometer consistency veto. The former uses a normalized spectrogram to check for spectral lines and nonstationary noise. The latter checks that the two-interferometer $\mathcal{F}$-statistic is greater than the value of either single-interferometer $\mathcal{F}$-statistic; failure of this condition strongly indicates a spectral line.

We found and fixed several bugs in the post-processing part of the pipeline. Their total effect on previous searches was negligible (the false dismissal rate of Ref. [9] was wrong by a few times 0.01%). However the effect on previous upper limits was more substantial, as described in the next section.

The O1 pipeline [9] corrected a bug in earlier versions [3,5] whereby the Doppler shift due to the Earth's orbital motion was omitted when applying detector-frame vetoes to candidate signals whose frequency is recorded in the solar system barycenter frame. However, we found that in the process the O1 pipeline introduced a bug in which $\dot{f}$ and $\ddot{f}$ were ignored when computing the frequency bands affected by the Fscan veto and removal of known lines. Although we did not remove known lines, we found that this bug fix reduced the number of candidate signals. This also means that the searches in Ref. [9] spuriously vetoed a fraction of the frequency band on the order of T_{span}/a for each search, of order a few times 10^{-4} for the worst case (SNR G1.9 + 0.3), increasing the false dismissal rate by about that (negligible) amount..

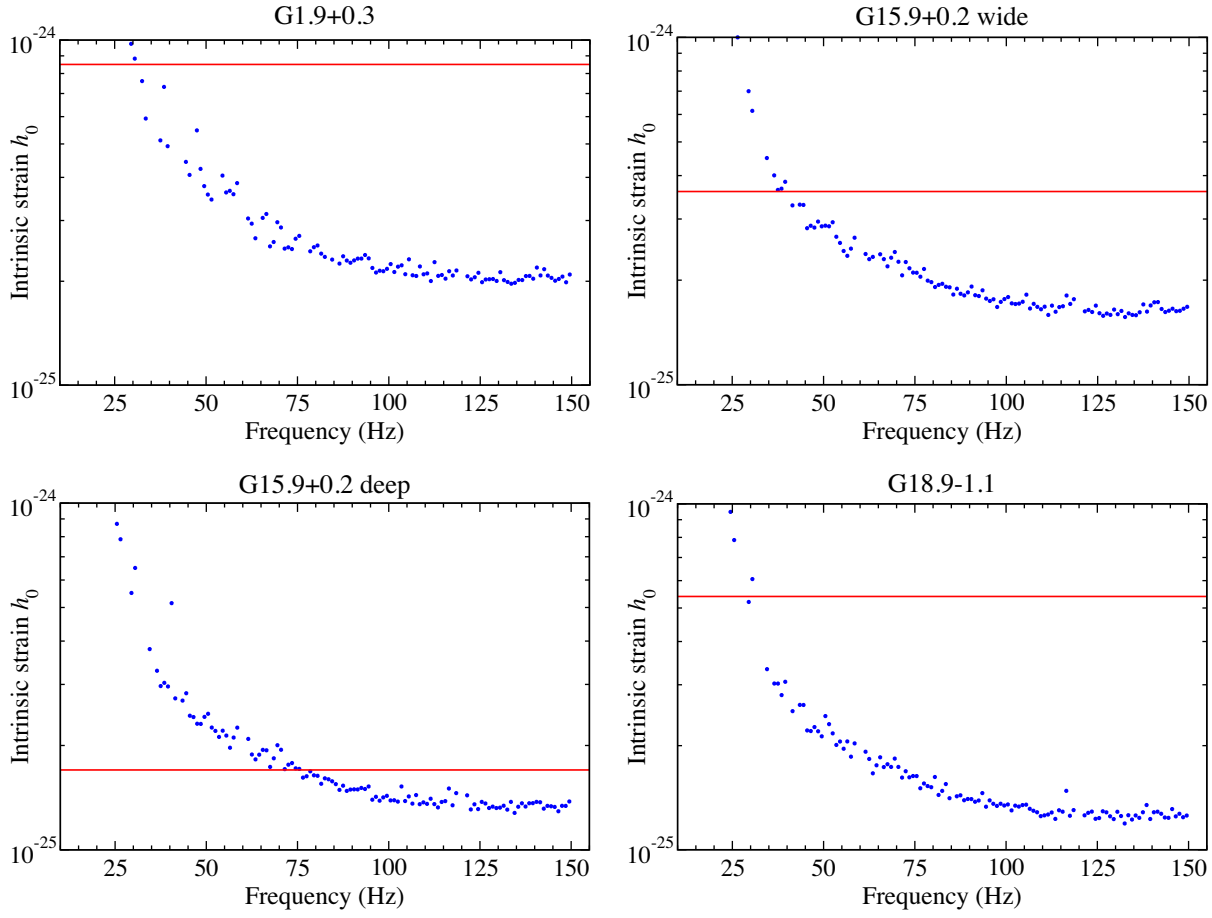

FIG. 1. Points represent the direct observational 90% confidence upper limits on the intrinsic strain h_0 as a function of frequency in 1 Hz bands for four searches. The (red) horizontal line indicates the indirect limit h_0^{age} from energy conservation. All figures trace a slightly distorted version of the noise curve.

When the $\dot{f}$-$\ddot{f}$ bug was fixed, it significantly increased the total frequency band vetoed in each search. As before, the veto criterion was very strict, including all templates whose detector-frame frequency ever came within eight SFT bins (almost 5 mHz) of an Fscan with sufficiently high power. (Eight bins was the width of the Dirichlet kernel used in computing the $\mathcal{F}$-statistic.) However, in the interest of setting upper limits on most frequency bands, we raised the power threshold (loosened the veto) from seven standard deviations to twenty. This brought the total vetoed band back down comparable to what it was in previous analyses such as Ref. [9]. As we shall see, this helped us set upper limits broadly without letting through an onerous number of candidate signals for manual inspection.

Unlike Ref. [9] we did not veto using the list of known instrumental lines [51]. With the $\dot{f}$-$\ddot{f}$ bug fixed, the total frequency band vetoed would have significantly reduced the number of upper limits we could set at high confidence. Also, we found that the search and bug-fixed Fscan veto performed quite well on most lines.

After these automated data-based vetoes were applied, the pipeline produced 21 search jobs whose loudest non-vetoed $\mathcal{F}$-statistic exceeded the 95% confidence threshold for Gaussian noise. We inspected all these candidates using the criteria from Ref. [9], essentially looking at the frequency spectrum of each candidate and the candidate's effect on the histogram of $\mathcal{F}$-statistic values.

No candidate survived visual inspection—all were much too broad-band compared to hardware-injected pulsar signals and had distorted histograms. Although we did not use the known lines as *a priori* vetoes, we checked *a posteriori* and found that most candidates were related to harmonics of 60 Hz or 0.5 Hz or to hardware-injected pulsar six, which was found (slightly Doppler shifted and broadened) in multiple searches at different sky locations. The O2 injected pulsar parameters are listed in Ref. [52]. Although it was loud, for many searches injected pulsar six was not loud enough to trigger the Fscan veto.

III. UPPER LIMITS

Having detected no signals, we placed upper limits on h_0 in 1 Hz bands using a procedure similar to Ref. [9]. That, is we estimated the h_0 that would be detected in each band (with the $\mathcal{F}$-statistic louder than the loudest actually recorded in that band) with a certain probability if the other signal parameters were varied randomly. This estimate used semi-analytical approximations to the $\mathcal{F}$-statistic probability

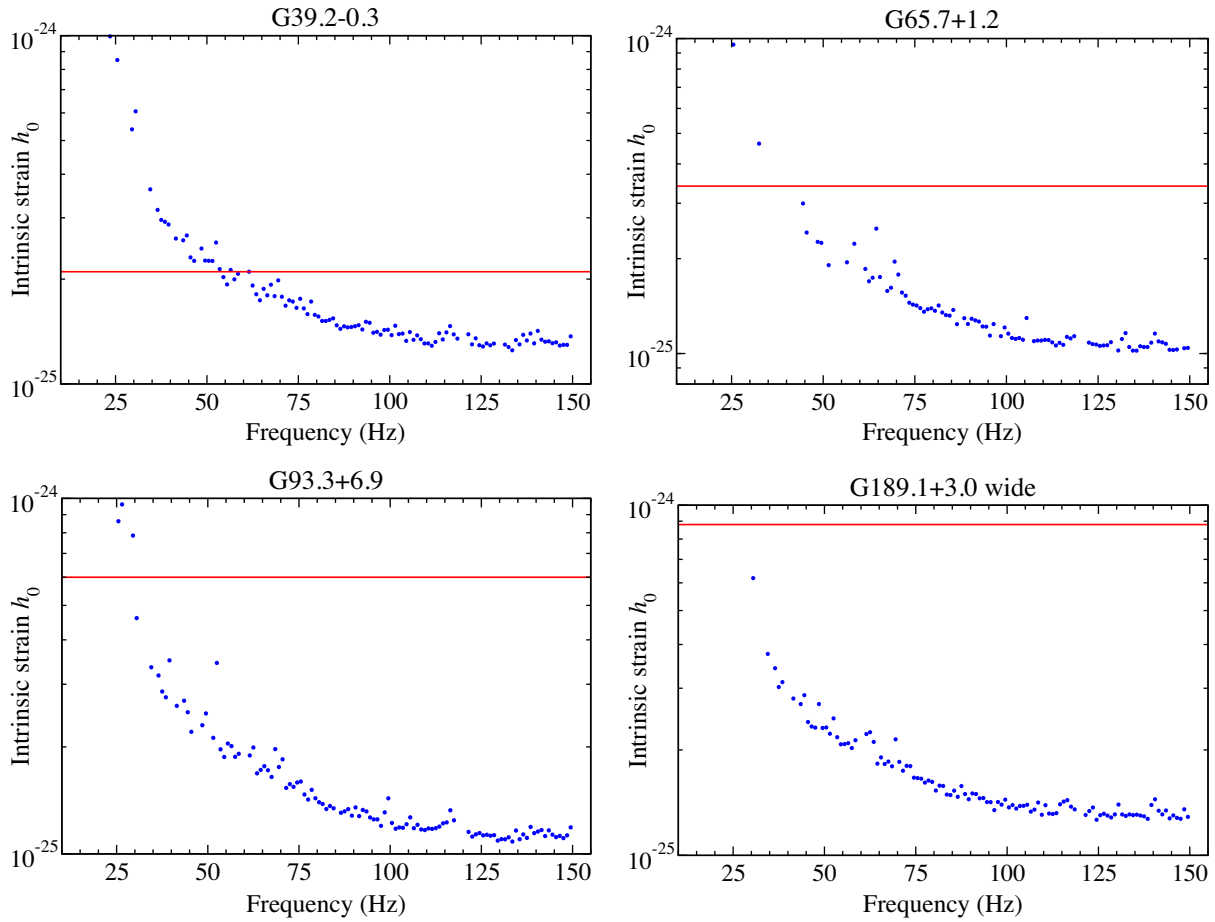

FIG. 2. Same as Fig. 1 for four additional searches.

distribution integrals and was spot-checked using one thousand software-injected signals per upper limit band.

Unlike [9], which set upper limits at 95% confidence, we reduced the confidence level to 90% (10% false dismissal). This was necessary to reduce the number of bands unsuitable for an upper limit. Upper limit bands were deemed unsuitable and dropped if more than 10% of the band was vetoed. We also dropped bands immediately adjoining 60 Hz and 120 Hz, the fundamental and first overtone of the electrical power mains. By spot checking the upper limit injections we found that, all else being equal, changing the confidence from 95% to 90% reduced the h_0 upper limits by 5%–8%. This difference is less than the calibration errors and negligible for the purposes of comparing to previous work.

Related to this, we found a bug in the O1 code whereby known line vetoes were not included in the total band veto. Since there were many known lines, this and the $\dot{f}$-$\ddot{f}$ bug meant that the vetoed band totals in Ref. [9] were often greatly underestimated. Strictly speaking, perhaps half of the 95% upper limit points should have been dropped. Or they should have used 90% confidence as we do here, which would have changed h_0 by a few percent.

The upper limits on h_0 which survived the veto check are plotted as a function of frequency in Figs. 1–4. Generally older targets produced better upper limits because longer integration times were possible for the fixed computational cost per target. The data files, including points not visible on the plots, are included in the supplemental material to this article [53]. In terms of the "sensitivity depth" defined in Ref. [54], these searches ranged from about 45 $\mathrm{Hz}^{-1/2}$ for young SNRs to 70 $\mathrm{Hz}^{-1/2}$ for older SNRs.

Upper limits on h_0 can be converted to upper limits on neutron star ellipticity ϵ using e.g., [2]

$$\epsilon \simeq 9.5 \times 10^{-5} \left(\frac{h_0}{1.2 \times 10^{-24}}\right) \left(\frac{D}{1\ \mathrm{kpc}}\right) \left(\frac{100\ \mathrm{Hz}}{f}\right)^2 \tag{5}$$

and to upper limits on a particular measure of r-mode amplitude α [55] using [56]

$$\alpha \simeq 0.28 \left(\frac{h_0}{10^{-24}}\right) \left(\frac{100\ \mathrm{Hz}}{f}\right)^3 \left(\frac{D}{1\ \mathrm{kpc}}\right). \tag{6}$$

The numerical values are uncertain by a factor of roughly two or three due to uncertainties in the unknown neutron star mass and equation of state.

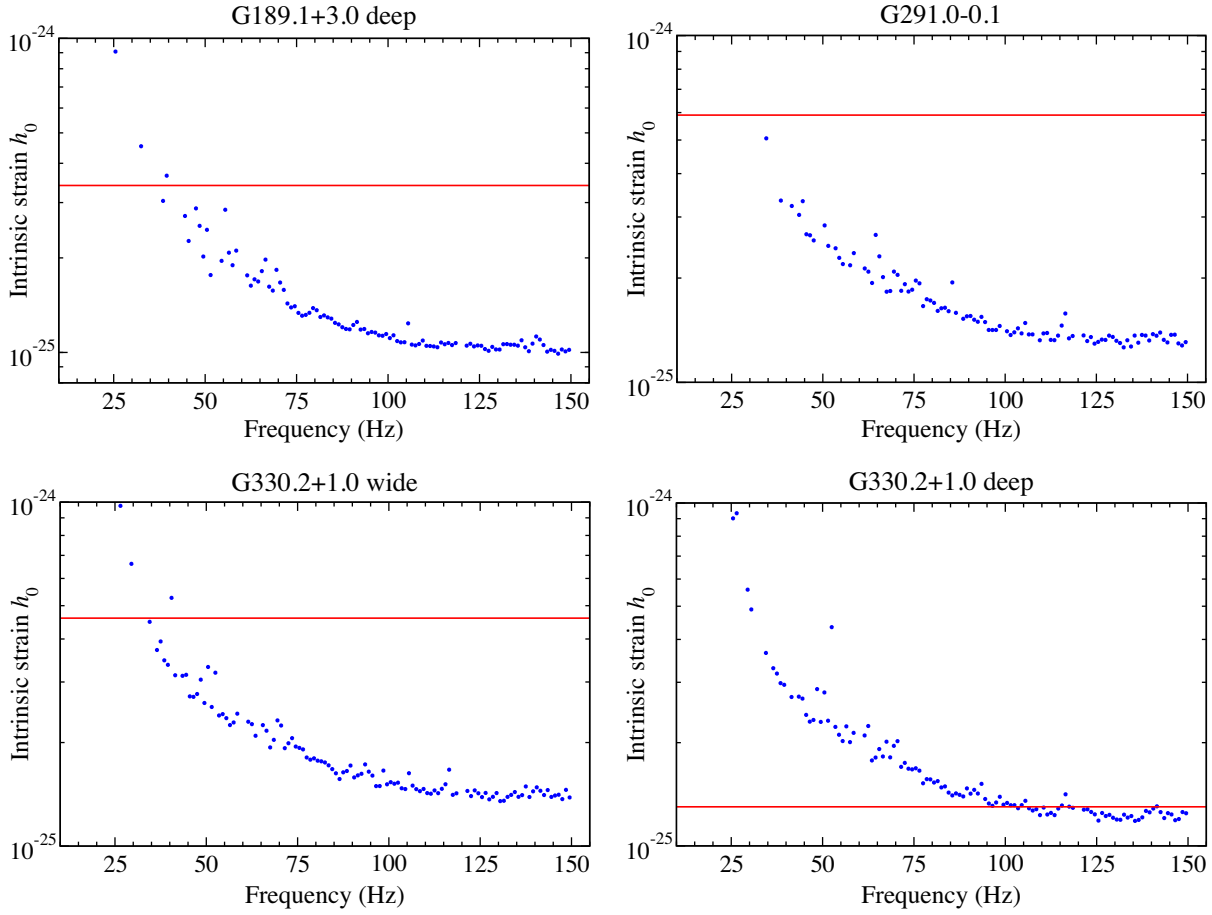

FIG. 3. Same as Fig. 1 for four additional searches.

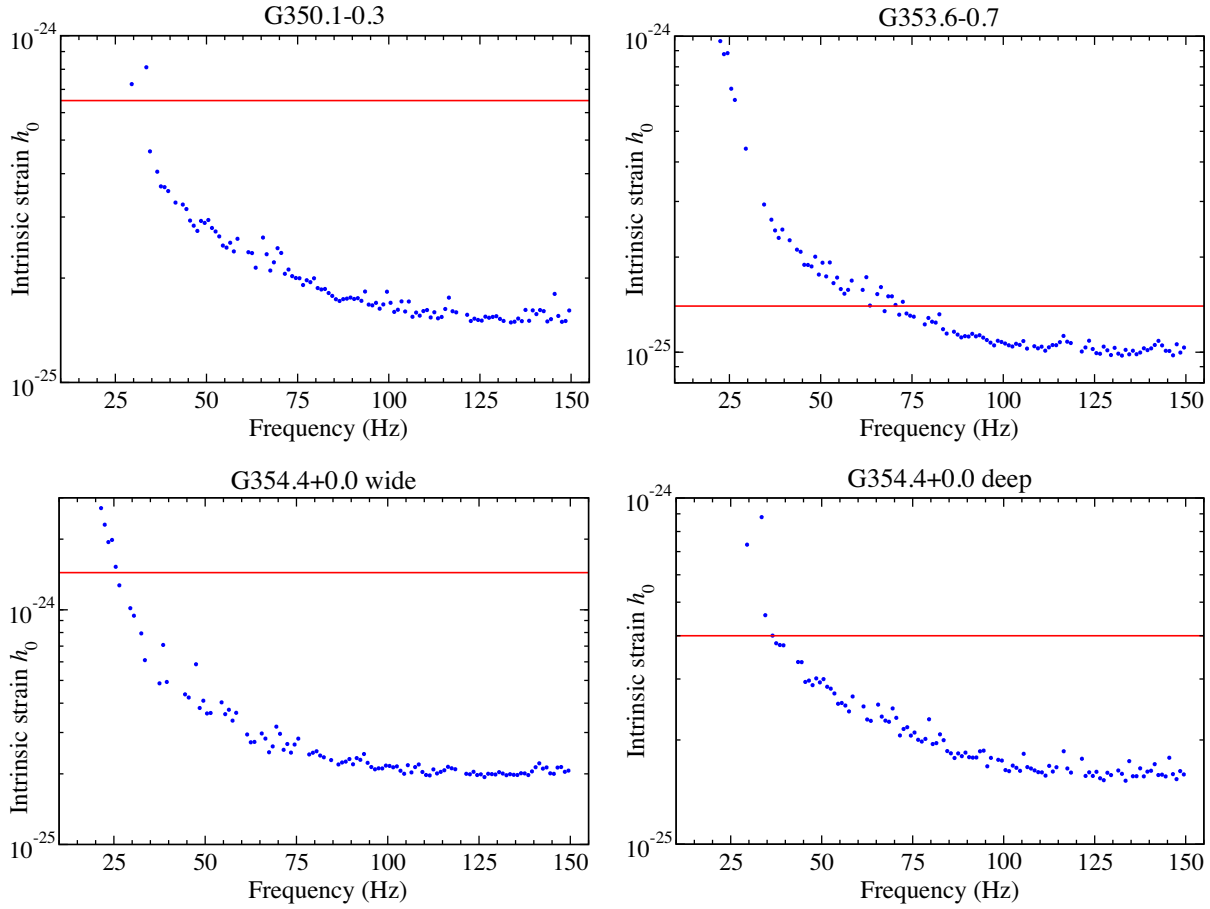

FIG. 4. Same as Fig. 1 for four additional searches.

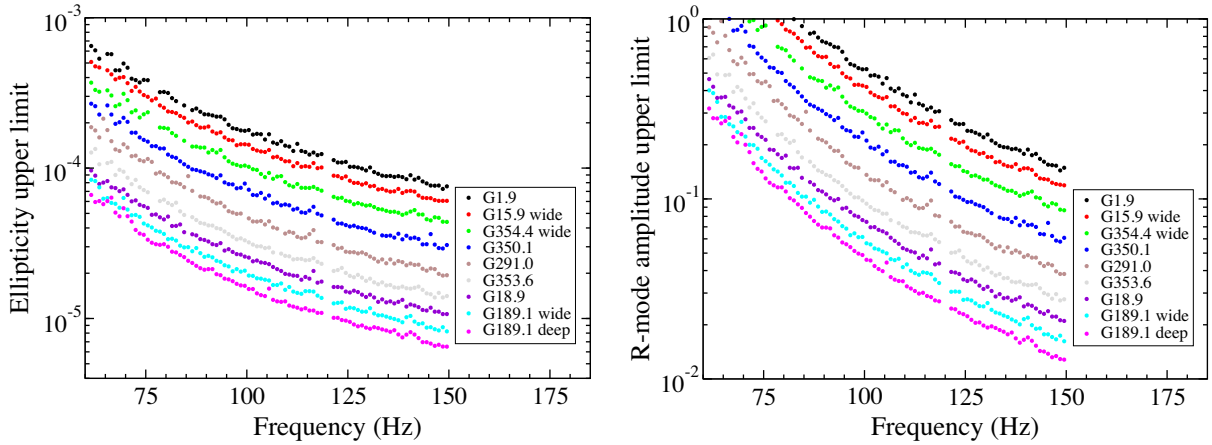

FIG. 5. Upper limits on fiducial neutron-star ellipticity (left panel) and r-mode amplitude (right panel) for a representative sample of SNRs. See the text for details.

We plot upper limits on ϵ for a selection of searches representing the range of these limits in the left panel of Fig. 5 and on α in the right panel. The differences between curves are primarily due to differences in the distances to the sources.

IV. DISCUSSION

Although we detected no signals, we placed the best upper limits yet on GW amplitude from these twelve SNRs. Our upper limits are as good (low) as 1.0×10^{-25}, and were generally about a factor of two better than similar limits on

the same SNRs using O1 data from Ref. [9]. Our upper limits are also (for several targets) up to a factor of two better than all-sky limits on O2 data from Ref. [52]. For SNR G1.9 + 0.3 our limits were about the same as Ref. [52] in our frequency band, but we covered five times the range of $\dot{f}$. Also, our searches included $\ddot{f}$ which is rare in the literature. Our searches included two new parameter sets for two of the SNRs. Part of the improved sensitivity over comparable O1 searches [9] was due to the reduced noise of O2 and part was due to our longer searches at lower frequencies, which seem to be characteristic of known young pulsars. Because of our focus on lower frequencies, our upper limits on neutron-star ellipticity and r-mode amplitude are less impressive than those from searches which extended to higher frequencies [9]. Our limits on r-mode amplitude do not reach the 10^{-3} level expected by the most detailed exploration of nonlinear saturation mechanisms [57]. But our ellipticity limits still in some cases approach a few times 10^{-6}, the rough maximum currently expected from normal neutron stars [58,59].

We are working on code to more efficiently handle high frequencies and long spin-down ages. With these improvements and ever improving strain noise from Advanced LIGO, the prospects for continuous GW detection will improve.

ACKNOWLEDGMENTS

This research has made use of data, software and/or web tools obtained from the Gravitational Wave Open Science Center (https://www.gw-openscience.org), a service of LIGO Laboratory, the LIGO Scientific Collaboration and the Virgo Collaboration. LIGO is funded by the U.S. National Science Foundation. Virgo is funded by the French Centre National de Recherche Scientifique (CNRS), the Italian Istituto Nazionale della Fisica Nucleare (INFN) and the Dutch Nikhef, with contributions by Polish and Hungarian institutes. This research was supported in part by NSF grants No. PHY-1604244, No. DMS-1620366, and No. PHY-1912419 to the University of California at San Diego; and by grant No. PHY-1912625 to Texas Tech University. The authors acknowledge computational resources provided by the High Performance Computing Center (HPCC) of Texas Tech University at Lubbock (http://www.depts.ttu.edu/hpcc/).

[1] K. Glampedakis and L. Gualtieri, Gravitational waves from single neutron stars: An advanced detector era survey, Astrophysics and Space Science Library **457**, 673 (2018).
[2] K. Wette *et al.*, Searching for gravitational waves from Cassiopeia A with LIGO, Classical Quantum Gravity **25**, 235011 (2008).
[3] J. Abadie *et al.*, First search for gravitational waves from the youngest known neutron star, Astrophys. J. **722**, 1504 (2010).
[4] J. Abadie, B. P. Abbott, R. Abbott, M. Abernathy, T. Accadia, F. Acernese, C. Adams, R. Adhikari, P. Ajith, B. Allen *et al.*, Directional Limits on Persistent Gravitational Waves Using LIGO S5 Science Data, Phys. Rev. Lett. **107**, 271102 (2011).
[5] J. Aasi, B. P. Abbott, R. Abbott, T. Abbott, M. R. Abernathy, F. Acernese, K. Ackley, C. Adams, T. Adams, P. Addesso *et al.*, Searches for continuous gravitational waves from nine young Supernova remnants, Astrophys. J. **813**, 39 (2015).
[6] L. Sun, A. Melatos, P. D. Lasky, C. T. Y. Chung, and N. S. Darman, Cross-correlation search for continuous gravitational waves from a compact object in SNR 1987A in LIGO Science run 5, Phys. Rev. D **94**, 082004 (2016).
[7] S. J. Zhu, M. A. Papa, H.-B. Eggenstein, R. Prix, K. Wette, B. Allen, O. Bock, D. Keitel, B. Krishnan, B. Machenschalk, M. Shaltev, and X. Siemens, Einstein@-Home search for continuous gravitational waves from Cassiopeia A, Phys. Rev. D **94**, 082008 (2016).
[8] B. P. Abbott, R. Abbott, T. D. Abbott, M. R. Abernathy, F. Acernese, K. Ackley, C. Adams, T. Adams, P. Addesso, R. X. Adhikari *et al.*, Directional Limits on Persistent Gravitational Waves from Advanced LIGO's First Observing Run, Phys. Rev. Lett. **118**, 121102 (2017).
[9] B. P. Abbott *et al.* (LIGO Scientific and Virgo Collaborations), Searches for continuous gravitational waves from 15 Supernova remnants and fomalhaut b with advanced LIGO, Astrophys. J. **875**, 122 (2019).
[10] J. Ming *et al.*, Results from an Einstein@Home search for continuous gravitational waves from Cassiopeia A, Vela Jr. and G347.3, Phys. Rev. D **100**, 024063 (2019).
[11] B. P. Abbott *et al.* (LIGO Scientific and Virgo Collaborations), Directional limits on persistent gravitational waves using data from Advanced LIGO's first two observing runs, Phys. Rev. D **100**, 062001 (2019).
[12] J. Aasi, J. Abadie, B. P. Abbott, T. Abbott, R. Abbott, M. R. Abernathy, T. Accadia, F. Acernese, C. Adams, T. Adams *et al.*, Directed search for continuous gravitational waves from the Galactic center, Phys. Rev. D **88**, 102002 (2013).
[13] O. J. Piccinni, P. Astone, S. D'Antonio, S. Frasca, G. Intini, I. La Rosa, P. Leaci, S. Mastrogiovanni, A. Miller, and C. Palomba, A directed search for continuous gravitational-wave signals from the Galactic center in Advanced LIGO second observing run, arXiv:1910.05097 [Phys. Rev. D (to be published)].
[14] B. P. Abbott, R. Abbott, T. D. Abbott, M. R. Abernathy, F. Acernese, K. Ackley, C. Adams, T. Adams, P. Addesso, R. X. Adhikari *et al.*, Search for continuous gravitational waves from neutron stars in globular cluster NGC 6544, Phys. Rev. D **95**, 082005 (2017).

[15] R. N. Manchester, G. B. Hobbs, A. Teoh, and M. Hobbs, The Australia telescope national facility pulsar catalogue, Astron. J. **129**, 1993 (2005).
[16] P. Jaranowski, A. Krolak, and B. F. Schutz, Data analysis of gravitational—wave signals from spinning neutron stars. 1. The signal and its detection, Phys. Rev. D **58**, 063001 (1998).
[17] C. Cutler and B. F. Schutz, The generalized F-statistic: Multiple detectors and multiple GW pulsars, Phys. Rev. D **72**, 063006 (2005).
[18] M. Vallisneri, J. Kanner, R. Williams, A. Weinstein, and B. Stephens, The LIGO open science center, J. Phys. Conf. Ser. **610**, 012021 (2015).
[19] R. Abbott *et al.* (LIGO Scientific and Virgo Collaborations), Open data from the first and second observing runs of Advanced LIGO and Advanced Virgo, arXiv:1912.11716.
[20] M. Cahillane, M. Hulko, J. S. Kissel *et al.*, LIGO Tech. Report No. LIGO-G1800319, 2018, https://dcc.ligo.org/LIGO-G1800319/public.
[21] D. A. Green, A revised catalogue of 294 Galactic supernova remnants, J. Astrophys. Astron. **40**, 36 (2019).
[22] S. Roy and S. Pal, Discovery of the small-diameter, young supernova remnant G354.4 + 0.0, Astrophys. J. **774**, 150 (2013).
[23] N. Hurley-Walker *et al.*, Candidate radio supernova remnants observed by the GLEAM survey over $345° < l < 60°$ and $180° < l < 240°$, Pub. Astron. Soc. Aust. **36**, e048 (2019).
[24] W. Reich, E. Fuerst, C. G. T. Haslam, P. Steffen, and K. Reif, A radio continuum survey of the Galactic Plane at 11 CM wavelength. I—The area L = 357.4 to 76 deg, B = −1.5 to + 1.5 deg, Astron. Astrophys. Suppl. Ser. **58**, 197 (1984).
[25] S. P. Reynolds, K. J. Borkowski, D. A. Green, U. Hwang, I. Harrus, and R. Petre, The youngest Galactic Supernova remnant: G1.9 + 0.3, Astrophys. J. Lett. **680**, L41 (2008).
[26] S. P. Reynolds, K. J. Borkowski, U. Hwang, I. Harrus, R. Petre, and G. Dubner, A new young Galactic Supernova remnant containing a compact object: G15.9 + 0.2, Astrophys. J. Lett. **652**, L45 (2006).
[27] R. Tüllmann, P. P. Plucinsky, T. J. Gaetz, P. Slane, J. P. Hughes, I. Harrus, and T. G. Pannuti, Searching for the Pulsar in G18.95-1.1: Discovery of an x-ray point source and associated synchrotron Nebula with Chandra, Astrophys. J. **720**, 848 (2010).
[28] I. M. Harrus, P. O. Slane, J. P. Hughes, and P. P. Plucinsky, An x-ray study of the Supernova remnant G18.95-1.1, Astrophys. J. **603**, 152 (2004).
[29] C. M. Olbert, J. W. Keohane, K. A. Arnaud, K. K. Dyer, S. P. Reynolds, and S. Safi-Harb, Chandra detection of a Pulsar wind Nebula associated with Supernova remnant 3C 396, Astrophys. J. Lett. **592**, L45 (2003).
[30] Y. Su, Y. Chen, J. Yang, B.-C. Koo, X. Zhou, D.-R. Lu, I.-G. Jeong, and T. DeLaney, Molecular environment and thermal x-ray spectroscopy of the semicircular young composite Supernova remnant 3C 396, Astrophys. J. **727**, 43 (2011).
[31] Z. Arzoumanian, S. Safi-Harb, T. L. Landecker, R. Kothes, and F. Camilo, Chandra confirmation of a Pulsar wind Nebula in DA 495, Astrophys. J. **687**, 505 (2008).
[32] R. Kothes, T. L. Landecker, and M. Wolleben, H I absorption of polarized emission: A new technique for determining kinematic distances to Galactic Supernova remnants, Astrophys. J. **607**, 855 (2004).
[33] R. Kothes, T. L. Landecker, W. Reich, S. Safi-Harb, and Z. Arzoumanian, DA 495: An aging Pulsar wind Nebula, Astrophys. J. **687**, 516 (2008).
[34] B. Jiang, Y. Chen, and Q. D. Wang, The Chandra view of DA 530: A subenergetic Supernova remnant with a Pulsar wind Nebula?, Astrophys. J. **670**, 1142 (2007).
[35] T. Foster and D. Routledge, A new distance technique for Galactic plane objects, Astrophys. J. **598**, 1005 (2003).
[36] C. M. Olbert, C. R. Clearfield, N. E. Williams, J. W. Keohane, and D. A. Frail, A bow shock Nebula around a compact x-ray source in the Supernova remnant IC 443, Astrophys. J. Lett. **554**, L205 (2001).
[37] R. A. Fesen and R. P. Kirshner, Spectrophotometry of the supernova remnant IC 443, Astrophys. J. **242**, 1023 (1980).
[38] R. Petre, A. E. Szymkowiak, F. D. Seward, and R. Willingale, A comprehensive study of the x-ray structure and spectrum of IC 443, Astrophys. J. **335**, 215 (1988).
[39] D. A. Swartz, G. G. Pavlov, T. Clarke, G. Castelletti, V. E. Zavlin, N. Bucciantini, M. Karovska, A. J. van der Horst, M. Yukita, and M. C. Weisskopf, High spatial resolution x-ray spectroscopy of the IC 443 Pulsar wind Nebula and environs, Astrophys. J. **808**, 84 (2015).
[40] P. Slane, J. P. Hughes, T. Temim, R. Rousseau, D. Castro, D. Foight, B. M. Gaensler, S. Funk, M. Lemoine-Goumard, J. D. Gelfand, D. A. Moffett, R. G. Dodson, and J. P. Bernstein, A broadband study of the emission from the composite Supernova remnant MSH 11-62, Astrophys. J. **749**, 131 (2012).
[41] D. Moffett, B. Gaensler, and A. Green, G291.0-0.1: Powered by a Pulsar? in Young Supernova Remnants: Eleventh Astrophysics Conference, edited by S. S. Holt and U. Hwang, *AIP Conference Prococeedings* Vol. 565 (AIP, Melville, NY, 2001), pp. 333–336.
[42] S. Park, K. Mori, O. Kargaltsev, P. O. Slane, J. P. Hughes, D. N. Burrows, G. P. Garmire, and G. G. Pavlov, Discovery of a candidate central compact object in the Galactic nonthermal SNR G330.2 + 1.0, Astrophys. J. **653**, L37 (2006).
[43] N. M. McClure-Griffiths, A. J. Green, J. M. Dickey, B. M. Gaensler, R. F. Haynes, and M. H. Wieringa, The southern Galactic plane survey: The test region, Astrophys. J. **551**, 394 (2001).
[44] S. Park, O. Kargaltsev, G. G. Pavlov, K. Mori, P. O. Slane, J. P. Hughes, D. N. Burrows, and G. P. Garmire, Nonthermal x-rays from Supernova remnant G330.2 + 1.0 and the characteristics of its central compact object, Astrophys. J. **695**, 431 (2009).
[45] K. Torii, H. Uchida, K. Hasuike, H. Tsunemi, Y. Yamaguchi, and S. Shibata, Discovery of a featureless x-ray spectrum in the Supernova remnant shell of G330.2 + 1.0, Publ. Astron. Soc. Jpn. **58**, L11 (2006).
[46] B. M. Gaensler, A. Tanna, P. O. Slane, C. L. Brogan, J. D. Gelfand, N. M. McClure-Griffiths, F. Camilo, C. Ng, and J. M. Miller, The (re-)discovery of G350.1-0.3: A young, luminous Supernova remnant and its neutron star, Astrophys. J. Lett. **680**, L37 (2008).

[47] I. Lovchinsky, P. Slane, B. M. Gaensler, J. P. Hughes, C.-Y. Ng, J. S. Lazendic, J. D. Gelfand, and C. L. Brogan, A Chandra observation of Supernova remnant G350.1-0.3 and its central compact object, Astrophys. J. **731**, 70 (2011).

[48] J. P. Halpern and E. V. Gotthelf, Two magnetar candidates in HESS Supernova remnants, Astrophys. J. **710**, 941 (2010).

[49] W. W. Tian, D. A. Leahy, M. Haverkorn, and B. Jiang, Discovery of the radio and x-ray counterpart of TeV γ-ray source HESS J1731-347, Astrophys. J. Lett. **679**, L85 (2008).

[50] LIGO Scientific Collaboration, LIGO Algorithm Library—LALSuite, free software (GPL)(2018).

[51] P. B. Covas, A. Effler, E. Goetz, P. M. Meyers, A. Neunzert, M. Oliver, B. L. Pearlstone, V. J. Roma, R. M. S. Schofield, V. B. Adya *et al.*, Identification and mitigation of narrow spectral artifacts that degrade searches for persistent gravitational waves in the first two observing runs of Advanced LIGO, Phys. Rev. D **97**, 082002 (2018).

[52] B. P. Abbott *et al.* (LIGO Scientific and Virgo Collaboration), All-sky search for continuous gravitational waves from isolated neutron stars using Advanced LIGO O2 data, Phys. Rev. D **100**, 024004 (2019).

[53] See Supplemental Material at http://link.aps.org/supplemental/10.1103/PhysRevD.101.083023. The data files included in the Supplemental Material are the upper limits we obtained for h_0 in each 1 Hz frequency bin for each of our searches. Bins where no upper limit was possible (due to the presence of a known detector line for example) are given the value $h_0 = 0.0$ in these files.

[54] C. Dreissigacker, R. Prix, and K. Wette, Fast and accurate sensitivity estimation for continuous-gravitational-wave searches, Phys. Rev. D **98**, 084058 (2018).

[55] L. Lindblom, B. J. Owen, and S. M. Morsink, Gravitational Radiation Instability in Hot Young Neutron Stars, Phys. Rev. Lett. **80**, 4843 (1998).

[56] B. J. Owen, How to adapt broad-band gravitational-wave searches for r-modes, Phys. Rev. D **82**, 104002 (2010).

[57] R. Bondarescu, S. A. Teukolsky, and I. Wasserman, Spinning down newborn neutron stars: Nonlinear development of the r-mode instability, Phys. Rev. D **79**, 104003 (2009).

[58] N. K. Johnson-McDaniel and B. J. Owen, Maximum elastic deformations of relativistic stars, Phys. Rev. D **88**, 044004 (2013).

[59] D. A. Baiko and A. I. Chugunov, Breaking properties of neutron star crust, Mon. Not. R. Astron. Soc. **480**, 5511 (2018).